Gradient Line Reaction Paths for Hindered Internal Rotation in H_2BNH_2 and Inversion in PF_3

Ruslan M. Minyaev,[†] David J. Wales,*,‡ and Tiffany R. Walsh[‡]

Institute of Physical and Organic Chemistry, Rostov State University, 194/2 Stachka Avenue, Rostov-on-Don 344090, Russian Federation, and University of Cambridge, University Chemical Laboratories, Lensfield Road, Cambridge CB2 1EW, U.K.

The potential energy surfaces of H_2NBH_2 and PF_3 in the regions of the hindered internal rotation in aminoborane and the inversion in trifluorophosphine have been studied in terms of the gradient line (steepest-descent) reaction pathways. We find that the gradient line reaction path for the aminoborane internal rotation consists of two equivalent paths separated in configuration space; the gradient line reaction path for the PF_3 inversion consists of three equivalent reaction paths. Hence, the aminoborane internal rotation and the AF_3 (A = P, S^+, Sb, As, Bi) inversion are fundamentally multidimensional processes.

Introduction

We have previously explored the utility of gradient line reaction paths[1] in analyzing potential energy surface (PES) topologies for molecular rearrangements and elucidating the corresponding reaction mechanisms.[2,3] In the present paper we employ the same approach to study the hindered internal rotation in aminoborane, H_2BNH_2, and the inversion in trifluorophosphine, PF_3. We define gradient lines as steepest-descent paths[4,5] in nonmass-weighted coordinates. Such paths are well-behaved mathematical objects that depend only upon the Born-Oppenheimer potential energy surface.

Aminoborane is the simplest molecule to exhibit dative N → B π-bonding.[6] The hindered internal rotation in this molecule has been studied by various semiempirical[7−9] and ab initio[10−17] methods. The first ab initio calculations revealed that upon rotation from the planar form, the nitrogen assumes a pyramidal conformation so that rigid rotation is not a valid assumption in this case.[10,11] More sophisticated ab initio calculations confirmed this conclusion.[15−17] However, the H_2BNH_2 PES topology and the aminoborane internal rotation mechanism still remain uncertain. In early work[10−14,16] the internal rotational pathway was thought to occur along a simple single-valley pathway. Ortiz[15] assumed the existence of two transition states with pyramidal nitrogen, but he did not study the H_2BNH_2 PES topology in the internal rotation region. In a recent paper[17] Allen and Fink, on the basis of high-level ab initio calculations, found that aminoborane has two rotational saddle points, one of C_s symmetry (with a pyramidal nitrogen) and one with C_{2v} symmetry (orthogonal configuration with planar nitrogen), although the second of these has two imaginary normal mode frequencies. Hence, the H_2BNH_2 PES in the configuration space of the internal rotation has a rather complicated topology. Here, we show that the gradient line reaction path of the aminoborane internal rotation consists of two equivalent reaction paths, **1a** ⇄ **2a** ⇄ **1b** and **1a** ⇄ **2b** ⇄ **1b** (see Scheme 1), separated in configuration space. H_2BNH_2 is equally likely to follow either one of these internal rotation paths, leading to a mechanism different from the commonly accepted one for rigid internal rotation. This means that the aminoborane internal rotation is

SCHEME 1
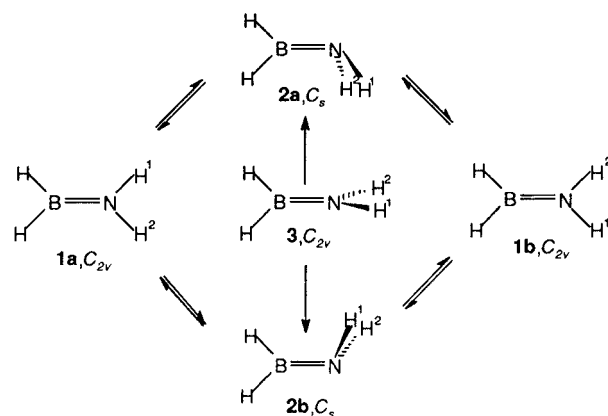
a multidimensional process that cannot really be adquately represented in one dimension.

AF_3 (A = P, S^+, Sb, As, Bi) molecules, **4−7**, seem to have
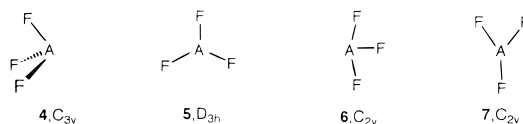
a more complicated PES topology than aminoborane in the internal rotation region. It has long been assumed that a planar D_{3h} structure, such as **5**, is the only possible transition state geometry for the inversion of various three-coordinated pyramidal C_{3v} structures.[18−25] However, several ab initio calculations[25−30] have produced surprising results. The pyramidal C_{3v} PF_3, SF_3^+, AsF_3, and SbF_3 molecules, **4**, invert through a T-shaped C_{2v} transition state **6** rather than through the D_{3h} structure **5**, which corresponds to an index three stationary point (three negative Hessian eigenvalues) on the corresponding PES. Further theoretical[31−34a] and experimental[30,37] investigations of the rearrangements of group 15 trivalent compounds corroborated the edge inversion of these compounds via the T-shaped structure.[34b] However, recently Gutsev[34b] found another C_{2v} Y-shaped structure, **7**, which, according to this author, is a more likely transition state for the PF_3 inversion than the T-shaped one. Clotet, Rubio, and Illas[31] noticed that the Y-shaped structure **7** is indeed a stationary point on the PF_3 PES but with two imaginary normal mode frequencies. Dixon,

Gradient Line Reaction Paths

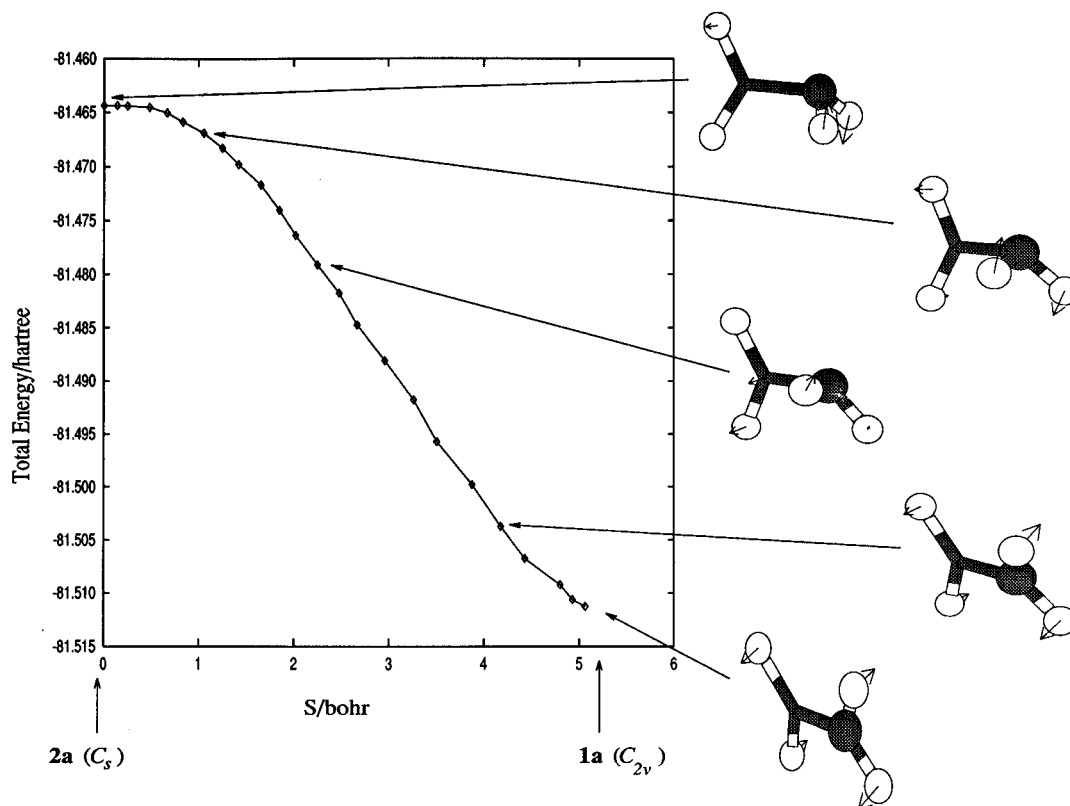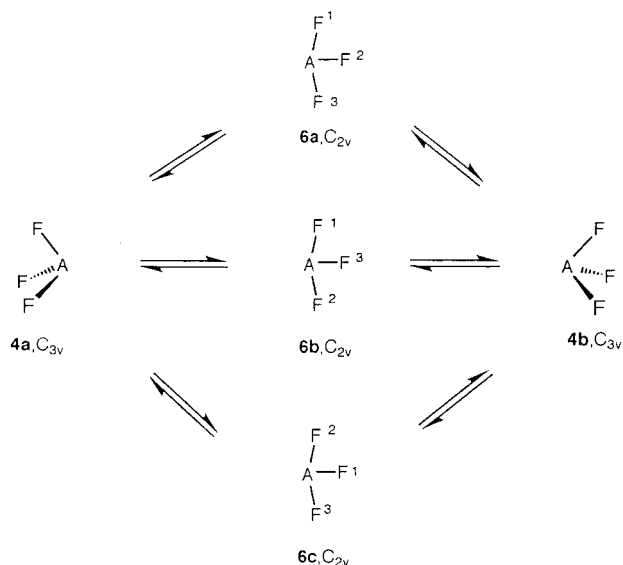*J. Phys. Chem. A, Vol. 101, No. 7, 1997* **1385**

Figure 1. Energy profile and evolution of the transition vector along the gradient line from **2a** to **1a** corresponding to the aminoborane internal rotation. S is the integrated path length in nuclear coordinate space. On the right is the evolution of the structure along this pathway. The arrows show the components of the reaction vector that corresponds to the transition vector of **2a** and to the smallest positive Hessian eigenvalue of **1a**. The shaded atom is nitrogen.

SCHEME 2

TABLE 1: Relative Energies (in kcal/mol) and the Number of Negative Hessian Eigenvalues (in Parentheses) Calculated for Stationary Points of Aminoborane at Different Levels of Theory

	structure			
method	**1**, C_{2v}	**2**, C_2	**3**, C_{2v}	ref
MP2/6-31G(d)	0 (0)	33.5 (1)	38.8 (2)	16
DZP/CISD	0 (0)	32.0 (1)	37.2 (2)	17
RHF/6-31G(d)	0 (0)	28.8 (1)	33.2 (2)	15
RHF/DZP	0 (0)	29.1 (1)	33.1 (2)	17
RHF/DZP	0 (0)	29.4 (1)	33.2 (2)	present work

TABLE 2: Relative Energies (in kcal/mol) and the Number of Negative Hessian Eigenvalues (in Parentheses) Calculated for Stationary Points of PF₃ at Different Levels of Theory

	structure			
method	**4a**, C_{3v}	**6**, C_{2v}	**5**, D_{3h}	ref
RHF/DZP	0 (0)	68.9 (1)	124.7 (3)	27
MP2/DZP	0 (0)	53.8 (1)	85.3 (3)	27
RHF/ECP	0 (0)	67.7 (1)		35
MP2/ECP	0 (0)	52.4 (1)		35
RHF/6-311G**	0 (0)	69.0 (1)		32
RHF/DZP	0 (0)	59.8 (1)	(3)	31
RHF/DZP	0 (0)	66.6 (1)	(3)	36
MP2/DZP	0 (0)	52.9 (1)	(3)	36
CASPT2/DZP	0 (0)	45.8 (1)	(3)	36
RHF/DZP	0 (0)	66.3 (1)	123.2 (3)	present work

Arduengo, and Fukunaga,[26] applying the microscopic reversibility principle, concluded that the PF₃ inversion process can occur in two degenerate ways. However, the D_{3h} structure **5** of AF₃ (A = P, S⁺, Sb, As, Bi) can distort into three equivalent C_{2v} T-shaped transition states, **6a**, **6b**, and **6c**, rather than into one or two, and all three permutational isomers must play an equivalent role in the inversion process (see Scheme 2).[26–32,36] Hence, we expect there to be three equivalent pathways **4a** ⇌ **6a** ⇌ **4b**, **4a** ⇌ **6b** ⇌ **4b**, and **4a** ⇌ **6c** ⇌ **4b** on the corresponding PES for the inversion process in AF₃ molecules. The existence of the three equivalent transition states reflects the complexity of the PES topology in AF₃ (A = P, S⁺, Sb,

As, Bi), which needs to be elucidated in order to correctly define the inversion mechanism.

In the present paper we study the PF₃ PES topology in the inversion region and show that the gradient line reaction path of the PF₃ inversion consists of three equivalent paths. This implies that, as in the case of the aminoborane internal rotation, the PF₃ inversion is really a multidimensional process and that the AF₃ (A = P, S⁺, Sb, As, Bi) PES for inversion can only be

1386 *J. Phys. Chem. A, Vol. 101, No. 7, 1997*

Minyaev et al.

TABLE 3: Total Energy (E_{tot} in hartree), Relative Energies (ΔE in kcal/mol),[a] the Number of the Negative Hessian Eigenvalues (λ), Dipole Moment (μ in debye), Bond Lengths (l in Å), and Bond Angles (in deg) Calculated at the RHF/DZP Level of Theory for Structures 1−3 of Aminoborane[b]

	structure		
value	**1**, C_{2v}	**2**, C_s	**3**, C_{2v}
E_{tot}	−81.51126	−81.46435	−81.51126
ΔE	0	29.4	33.2
λ	0	1	2
μ	1.758 (1.844)	1.619	0.972
l(BN)	1.395 (1.391)	1.472	1.459
l(BH)	1.193 (1.195)	1.195	1.202
l(BH)	1.193 (1.195)	1.203	1.202
l(NH)	0.995 (1.004)	1.006	0.994
HBH	121.3 (122.2)	117.8	116.8
HNH	114.0 (114.2)	104.3	114.1

[a] 1 hartree = 627.5095 kcal/mol. [b] The experimental values[42a,43−45] are given in parentheses.

TABLE 4: Total Energy (E_{tot} in hartree), Relative Energies (ΔE in kcal/mol),[a] the Number of the Negative Hessian Eigenvalues (λ), Dipole Moment (μ in debye), Bond Lengths (l in Å), and Bond Angles (in deg) Calculated at the RHF/DZP Level of Theory for Structures 4−7 of Trifluorophosphine

	structure			
value	**4**, C_{3v}	**5**, D_{3h}	**6**, C_{2v}	**7**, C_{2v}
E_{tot}	−639.21228	−639.01598	−639.10657	−639.03078
ΔE	0	123.2	66.3	113.9
λ	0	3	1	2
μ	1.563 (1.030)[b]	0	0.834	1.970
l(PF$_a$)	1.560 (1.561)[b]	1.660	1.630	1.836
l(PF$_e$)	1.560 (1.561)[b]	1.660	1.550	1.584
F$_a$PF$_a$	97.2 (97.7)[b]	120.0	172.8	133.3
F$_a$PF$_e$	97.2 (97.7)[b]	120.0	86.4	93.3

[a] 1 hartree = 627.5095 kcal/mol. [b] The experimental values[50] are given in parentheses.

correctly described by at least three internal coordinates. Such an approach is required to calculate tunneling splittings for low-energy rearrangements such as the BiF$_3$ inversion.

Method

All the stationary point optimization calculations in this work were performed by standard restricted Hartree−Fock calculations with double zeta plus polarization basis sets (RHF/DZP)[38] using the CADPAC[39] program and employing analytic first and second derivatives at every step. The geometric parameters, the Hessian index, λ (hereafter, λ designates the number of the

negative Hessian eigenvalues), and the relative energies for the aminoborane **1**−**3** and trifluorophosphine structures **4**−**6** calculated in the present work at the RHF/DZP level agree with those obtained by higher-level ab initio calculations (see Tables 1 and 2).[28−32,35,36] The PES topology of these systems in the region of these rearrangements is not affected by larger basis sets or correlation energy.[28−32,35,36] Hence, we employ the relatively low-cost RHF/DZP approach to study the rearrangement mechanisms in the present work.

The CADPAC derivatives were used in geometry optimization and pathway calculations by our program OPTIM, which is based upon eigenvector-following in Cartesian coordinates. Details of the precise algorithm employed can be found
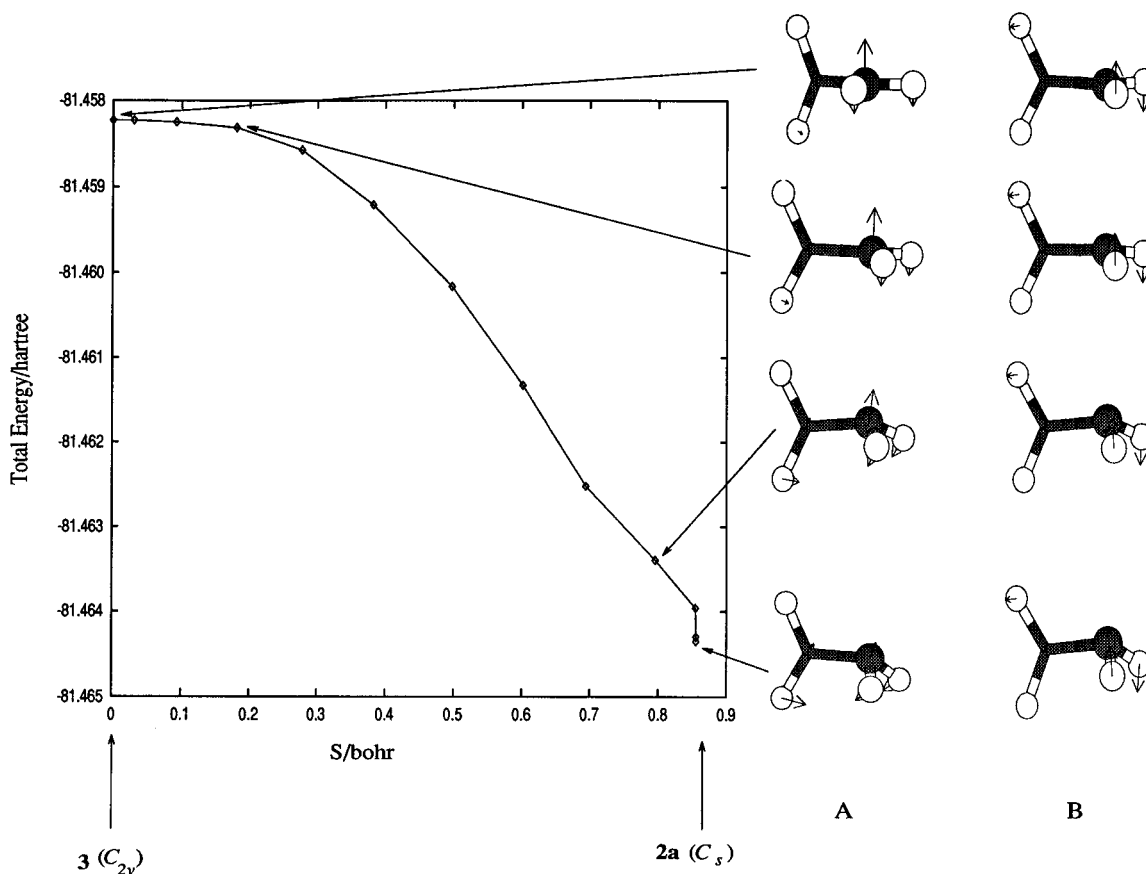

Figure 2. Energy profile (left) and evolution of the two Hessian eigenvectors (right) corresponding to the two negative eigenvalues of structure **3** for the gradient line from index two saddle **3** to transition state **2a**. The other side of the path from **3** to **2b** is analogous. S is the integrated path length in nuclear coordinate space. **B** is the Hessian eigenvector of **3** which correlates with the transition vector of **2a** and corresponds to the smallest magnitude negative eigenvalue of **3**. The other Hessian eigenvector, **A**, corresponds to the lowest Hessian eigenvalue of **3**, which correlates with the smallest positive eigenvalue of **2a**. Arrows designate the atomic components of the Hessian eigenvectors.

Gradient Line Reaction Paths

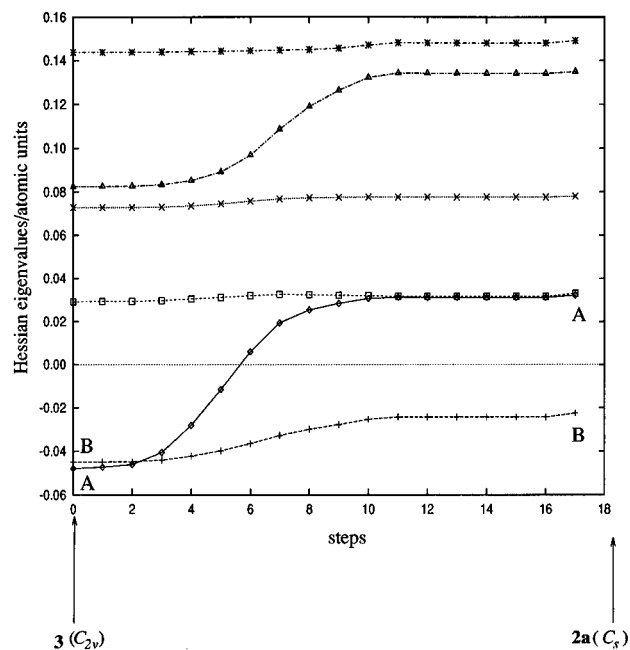*J. Phys. Chem. A, Vol. 101, No. 7, 1997* **1387**

Figure 3. Evolution of the six lowest eigenvalues of the projected Hessian (nonmass-weighted) along the approximate gradient line from **3** to **2a** as determined by overlap of the corresponding Hessian eigenvectors. The eigenvector-following steps correspond to the points in Figure 2. The smallest negative eigenvalue (left) smoothly transforms into the smallest positive eigenvalue (right), and the other negative eigenvalue (left) correlates with the unique negative eigenvalue (right). The evolution of the eigenvalues along the gradient line from **3** to **2b** is a mirror image.
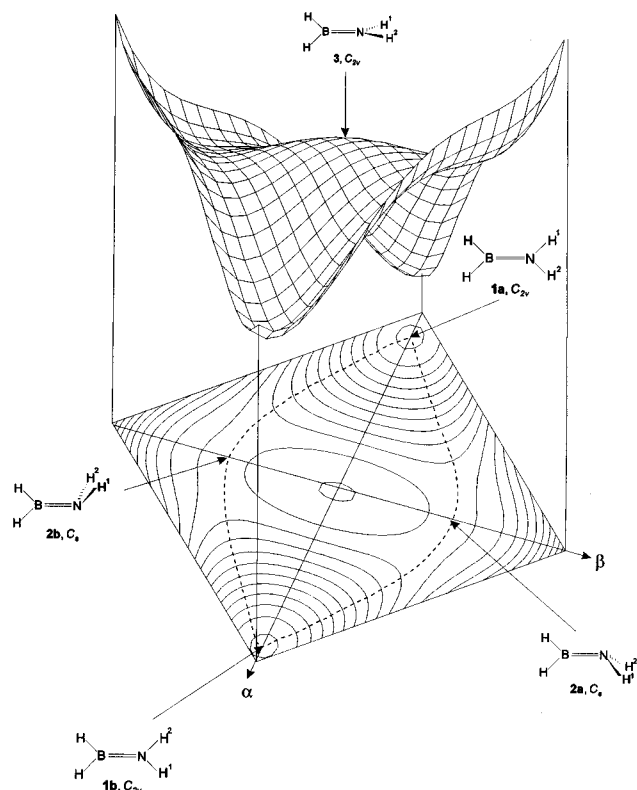

Figure 4. Schematic three-dimensional representation of the H_2BNH_2 PES (above) and its two-dimensional projection (below) in the region of the aminoborane internal rotation. The dashed lines indicate the two equivalent gradient lines linking **1a** to **1b** via transition states **2a** and **2b**. The gradient lines corresponding to the two negative Hessian eigenvalues of **3** are the perpendicular solid lines.
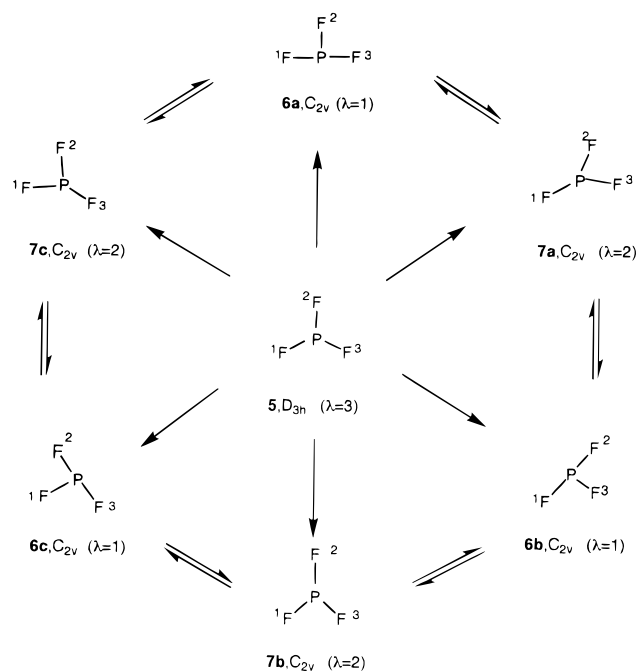

Figure 5. Distribution of stationary points in the restricted planar configuration space of PF_3.

elsewhere.[40] Convergence was considered to have been achieved when the root mean square force was less than 10^{-6} atomic units and the largest unscaled step was less than 0.005 bohr. These conditions generally reduce the six "zero" Hessian eigenvalues to less than 1 cm^{-1} in magnitude. The basis sets employed were those supplied in the standard CADPAC library.[39,41]

Stationary Points on the H_2BNH_2 PES

According to our calculations, structures **1** (C_{2v}), **2** (C_s), and **3** (C_{2v}) correspond to a minimum ($\lambda = 0$), a transition state ($\lambda = 1$), and an index two ($\lambda = 2$) saddle point, respectively. The calculated energies and geometrical parameters of **1**, **2**, and **3** are listed in Table 3 and are in good agreement with previous ab initio calculations.[10−17]

In structure **1**, the boron atom forms a π-dative (donor−acceptor)[6] bond with the nitrogen atom. When the BH_2 fragment is twisted through 90° into an orthogonal C_{2v} form **3** or into C_s configuration **2** with a pyramidal nitrogen, the π-dative NB bond is broken, thus increasing the BN distance in **2** and **3** compared to **1**. Two enantiomeric C_s structures, **2a** and **2b**, are true transition state structures[5] with a calculated energy barrier of 29.4 kcal/mol for the aminoborane internal rotation. This energy barrier appears to be in reasonable agreement with the experimental activation barrier to internal rotation obtained by ${}^1H$ NMR spectroscopy for various substituted aminoboranes, which ranges from 17 to 27 kcal/mol.[42]

Structure **3** (C_{2v}) might be considered a "transition state" for the "inversion process" at nitrogen between the two enantiomeric structures **2a** and **2b**. However, it is not a true transition state in the Murrell−Laidler sense[5] because it has two negative Hessian eigenvalues.

Internal Rotation Pathway in H_2BNH_2

The internal rotation pathway (gradient line reaction path) in H_2BNH_2 consists of two parts. Employing the eigenvector-following[47−49] method with starting displacements parallel and antiparallel to the transition vector of **2a**, we calculated the pathway and energy profile as well as the evolution of the transition vector along one of these paths between mimima **1a** and **1b**. The part connecting **2a** to **1a** is shown in Figure 1.
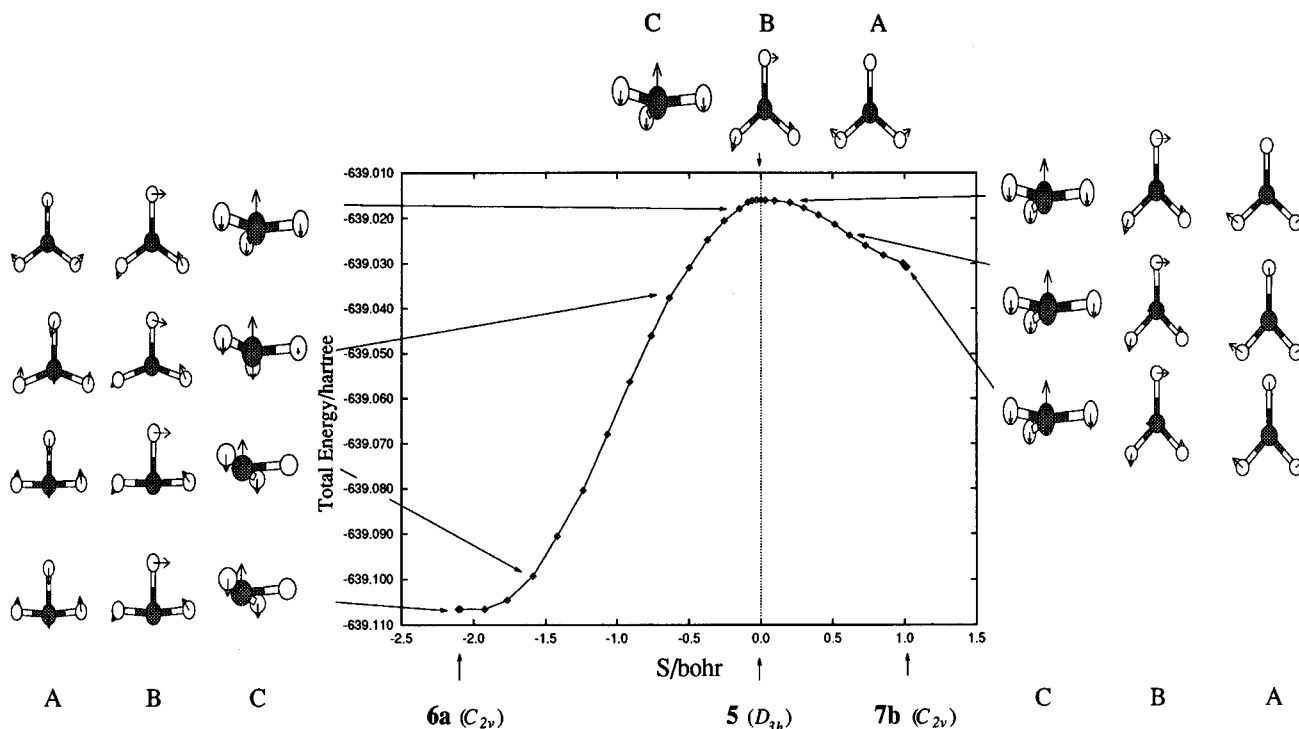
Figure 6. Energy profile and evolution of the three Hessian eigenvectors corresponding to the three negative Hessian eigenvalues of **5** along the gradient line connecting this structure to transition state **6a** and to the index two saddle point **7b**. *S* is the integrated path length in nuclear coordinate space. **C** is the Hessian eigenvector of **5** which correlates with the transition vector of **6a**, and **A** is the Hessian eigenvector which correlates with the Hessian eigenvector corresponding to the smallest positive eigenvalue of **6a**.
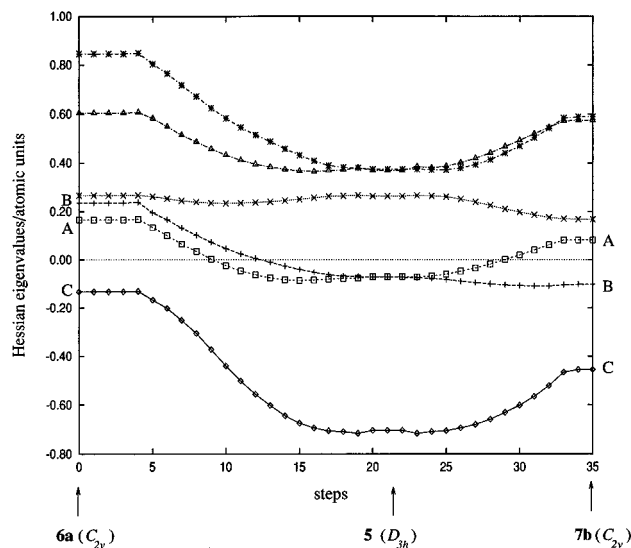

Figure 7. Evolution of the six lowest eigenvalues of the projected Hessian (nonmass-weighted) along the approximate gradient line from saddle point **5** to transition state **6a** and to **7b** as determined by overlap of the corresponding Hessian eigenvectors. The eigenvector-following steps correspond to the points in Figure 6.

The above pathway is not an exact gradient line, since the eigenvector-following steps are not strictly parallel to the gradient vector.[47-50] However, it is close enough for the present purposes and has the same symmetry properties.

To prove that the gradient line reaction path of the aminoborane internal rotation consists of two equivalent pathways, we calculated the energy profile and the evolution of the two Hessian eigenvectors corresponding to negative Hessian eigenvalues along the gradient lines emanating from the index two saddle point **3**. Figures 2 and 3 summarize the results obtained on following the gradient line, which correlates with displacements along the eigenvector corresponding to the most negative

Hessian eigenvalue of structure **3**. Figure 2 shows the pathway from index two saddle **3** to transition state **2a**, as well as the evolution of the two lowest Hessian eigenvectors along the path. In Figure 2 one can see that the Hessian eigenvector corresponding to the smallest negative Hessian eigenvalue of **3** transforms smoothly into the Hessian eigenvector with the smallest positive eigenvalue of transition state **2a**, whereas the Hessian eigenvector corresponding to the other negative eigenvalue of **3** transforms into the transition vector at **2a**. In Figure 3, evolution of the six lowest Hessian eigenvalues is shown along the pathway from **3** to **2a**. The eigenvalues plotted in Figure 3 are for the nonmass-weighted Hessian with overall rotation and translation projected out.[47g] The correct correlation was ensured by evaluating the overlap between all the Hessian eigenvectors at consecutive steps. Gradient lines terminate only at stationary points on a PES.[1,4] Hence, there are probably no stationary points other than **1a**, **1b**, **2a**, **2b**, and **3** on the H_2-BNH_2 PES in the region of the aminoborane internal rotation. This mechanism therefore corresponds to two distinct valleys beginning at one minimum **1a**, circumnavigating the hill **3**, and then ending at the other minimum **1b**. The schematic three-dimensional shape of the H_2BNH_2 PES and its projection are depicted in Figure 4. Thus, the internal hindered rotation in aminoborane is a multidimensional process that can only be correctly described by at least two internal coordinates: the rotation angle about the BN bond and the inversion angle at the nitrogen center.

The observed topology of the H_2BNH_2 PES may be quite common for the internal rotation of various organic and inorganic systems, particularly those with two equivalent rotors.

Stationary Points on the PF$_3$ PES

According to our calculations, structures **4** (C_{3v}), **5** (D_{3h}), **6** (C_{2v}), and **7** (C_{2v}) correspond to a minimum ($\lambda = 0$), an index three ($\lambda = 3$) stationary point, a transition state ($\lambda = 1$), and an index two ($\lambda = 2$) stationary point on the PF$_3$ PES, respectively.

Gradient Line Reaction Paths

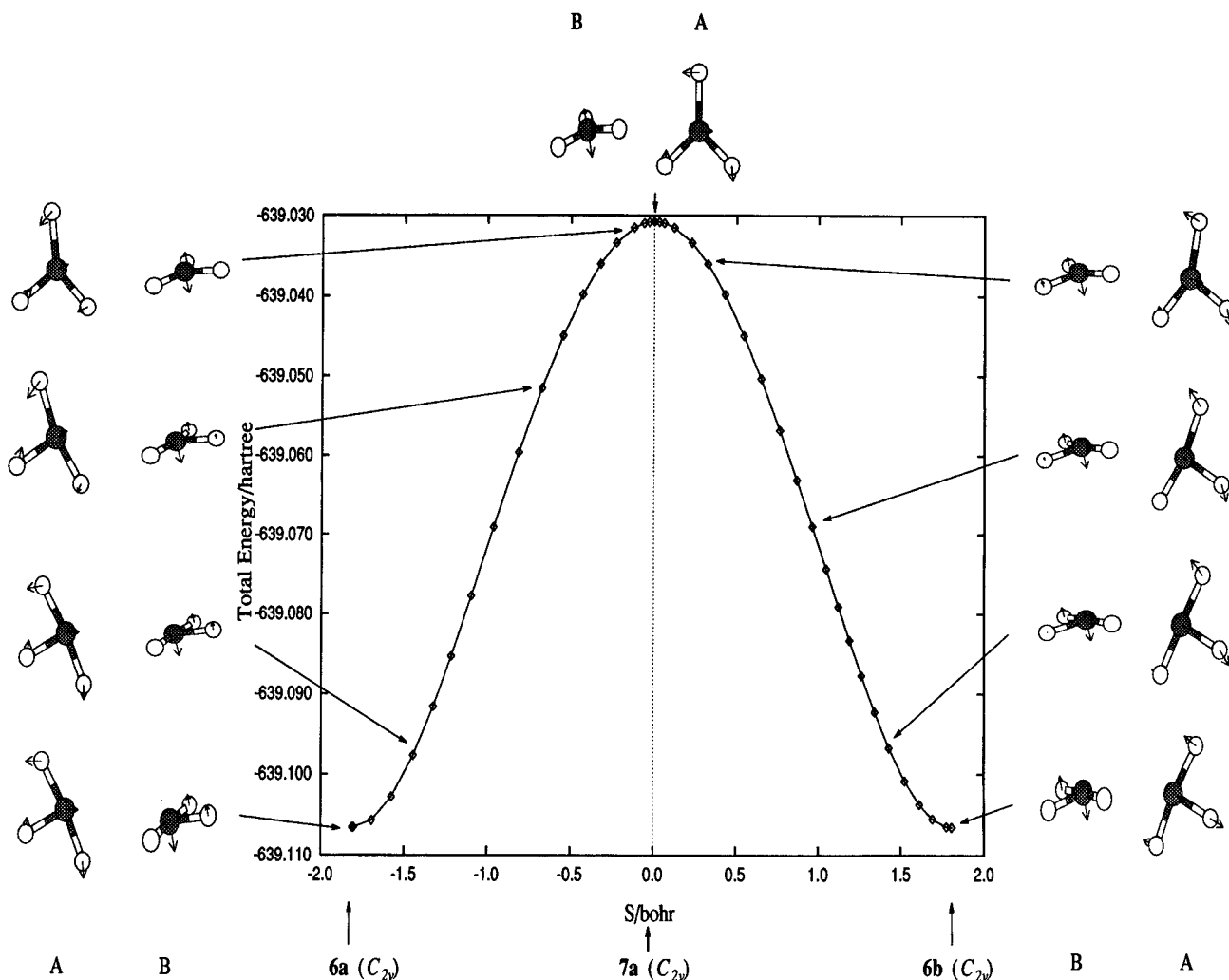*J. Phys. Chem. A, Vol. 101, No. 7, 1997* **1389**

Figure 8. Energy profile and evolution of the two Hessian eigenvectors of **7a** corresponding to negative Hessian eigenvalues along the gradient line from the index two saddle point **7a** to transition states **6a** and **6b**. S is the integrated path length in nuclear coordinate space. **A** is the Hessian eigenvector of **7a** which correlates with the transition vector of **6a**, and **B** correlates with the eigenvector corresponding to the smallest positive eigenvalue of **6a**.

Calculated energies and geometrical parameters of structures **4**−**7** are listed in Table 4 and are in good agreement with previous ab initio calculations[25−36] and available experimental data.[51] On the PF_3 PES there are three equivalent transition states, **6a**, **6b**, and **6c**, and three equivalent index two saddles **7a**, **7b**, and **7c**. The molecular structure of **6a**, **6b**, and **6c** is a T-shaped C_{2v} configuration with different axial and equatorial PF bond lengths of 1.630 and 1.550 Å, respectively. The axial fluorines have a larger negative charge than the equatorial fluorine according to Mulliken population analysis. These data are in agreement with the polarity rule for bisphenoid structures.[52]

The stationary point distribution in the neighborhood of planar PF_3 is shown schematically in Figure 5. To prove that this topology is correct, we consider the network of gradient lines connecting all the stationary points and the evolution of the Hessian eigenvectors and eigenvalues along these lines. The energy profile and evolution of the three Hessian eigenvectors corresponding to the negative eigenvalues in structure **5** along the gradient lines emanating from the index three saddle **5** toward transition state **6a** and toward the index two saddle **7b** are presented in Figure 6. The two Hessian eigenvectors corresponding to the degenerate negative Hessian eigenvalue of **5** split apart and convert smoothly into the Hessian eigenvectors corresponding to the two smallest positive eigenvalues of **6a**. The Hessian eigenvector corresponding to the most
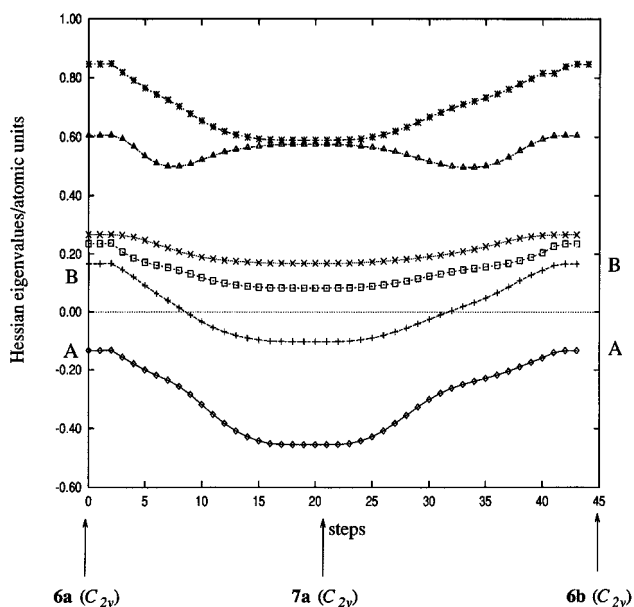

Figure 9. Evolution of the six lowest eigenvalues of the projected Hessian (nonmass-weighted) along the approximate gradient line from point **7a** to transition states **6a** and **6b** as determined by overlap of the corresponding Hessian eigenvectors. The eigenvector-following steps correspond to the points in Figure 8.
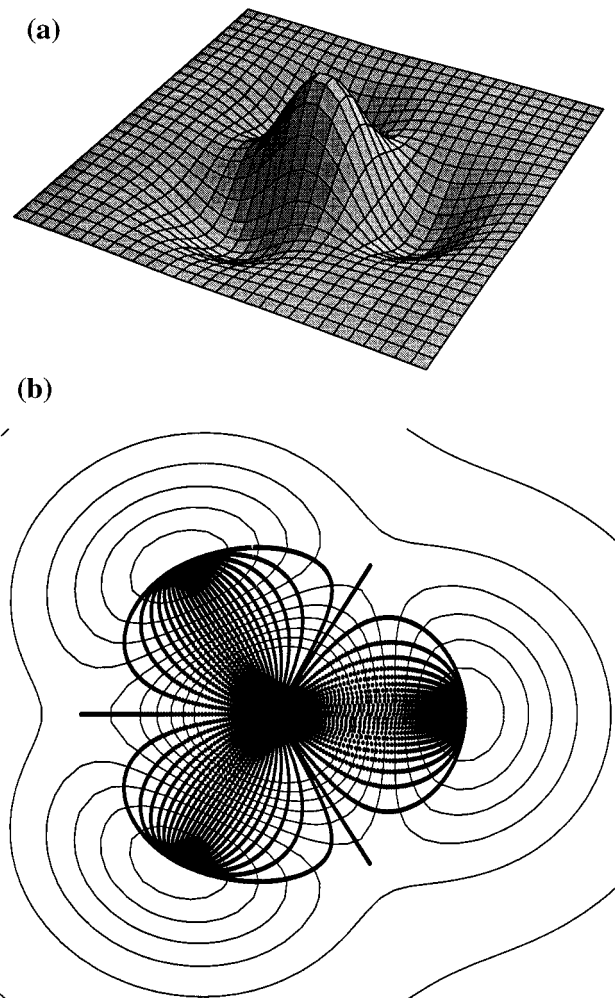
(a)

(b)

Figure 10. Surface (a) and its contour and gradient lines (b) for the simple analytic function, which mirrors the topology of the PF_3 PES in the region of the planar configuration (see Figure 5). The gradient lines are shown by bold lines. An infinite number of gradient lines connect point **5** to each "minimum" **6a**, **6b**, **6c**, while only three gradient lines connect **5** to **7a**, **7b**, and **7c**.

negative eigenvalue of **5** transforms into the transition vector of **6a**. On the gradient line from **5** to **7b**, one of these three eigenvectors of **5** changes into the Hessian eigenvector corresponding to the smallest positive eigenvalue and the other two become the two eigenvectors corresponding to the negative Hessian eigenvalues. Figure 7 shows the evolution of the six lowest eigenvalues of the projected nonmass-weighted Hessian along the approximate gradient line from **5** to **6a** and from **5** to **7b**. The energy profile and evolution of the Hessian eigenvectors and eigenvalues along gradient lines from **7a** to **6a** and **6b** are shown in Figures 8 and 9. The Hessian eigenvector corresponding to the smallest negative eigenvalue of **7a** converts into the transition vector for both **6a** and **6b**. The eigenvector corresponding to the other negative eigenvalue of **7a** changes into the eigenvector corresponding to the smallest positive Hessian eigenvalue for both **6a** and **6b**. This correlation is confirmed by the evolution of the five lowest Hessian eigenvalues (see Figure 9). We have also obtained the corresponding correlations for the other stationary points. Gradient lines terminate only at stationary points,[1,4] and to illustrate this, we calculated the gradient lines for a simple analytic function that mirrors the topology of the planar PF_3 PES (Figure 10). An infinite number of gradient lines emanating from the three minima **6a**, **6b**, and **6c** terminate at point **5**, while only three gradient lines connect point **5** with the index two points **7a**,
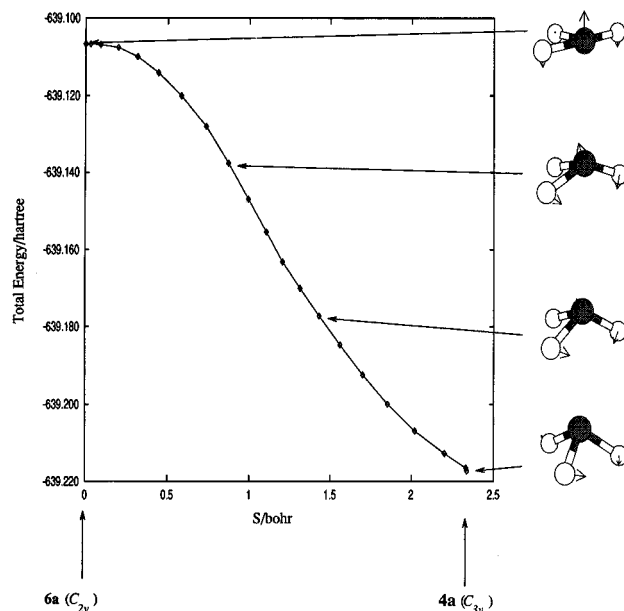

Figure 11. Energy profile and evolution of the transition vector along the reaction path corresponding to the PF_3 inversion. S is the integrated path length in nuclear coordinate space.
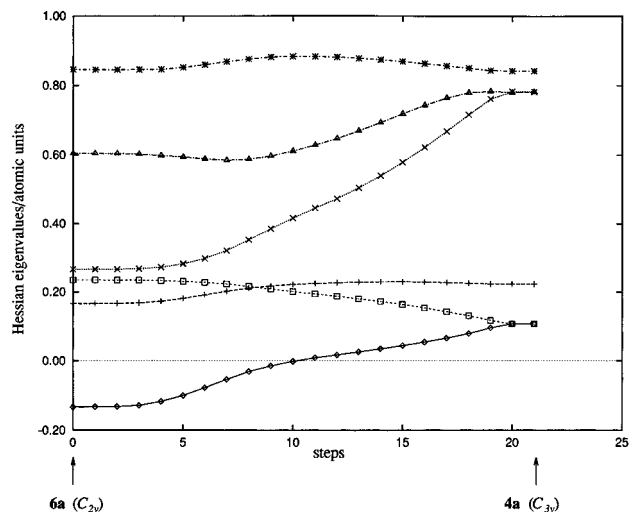

Figure 12. Evolution of the six lowest eigenvalues of the projected Hessian (nonmass-weighted) along the appropriate gradient line from the transition state **6a** to the minimum **4a** as determined by the overlap of the corresponding Hessian eigenvectors. The eigenvector-following steps correspond to the points in Figure 11.

7b, and **7c**. Gradient lines connecting structures **6** and **7** are omitted for clarity. Hence, the gradient line network presented in Figure 5 (and also in Figure 10) indicates that there are probably no stationary points other than **4**, **5**, **6a**, **6b**, **6c**, **7a**, **7b**, and **7c** in this region. In a restricted space corresponding to planar configurations of PF_3 the pathway **6a** $\rightleftarrows$ **7a** $\rightleftarrows$ **6b** $\rightleftarrows$ **7b** $\rightleftarrows$ **6c** $\rightleftarrows$ **7c** $\rightleftarrows$ **6a** might be considered the "pseudorotation" path for the T-shaped structure **6**, where structure **7** would correspond to a "transition state". However, **7** is not a true transition state in the Murrell−Laidler sense[5] because it has two negative Hessian eigenvalues. The PF_3 PES topology in this restricted space is probably common to molecules with a T-shaped C_{2v} minimum energy structure. For example, EF_3 (E = Cl, Br, I, At),[53,54] $BrCl_3$, and AF_3^- (A = P, Sb, As, Bi)[55,56] all have T-shaped C_{2v} minima. If a D_{3h} structure is not a minimum on the corresponding PES for these molecules, then it may be an index two saddle point. Then the PES of these
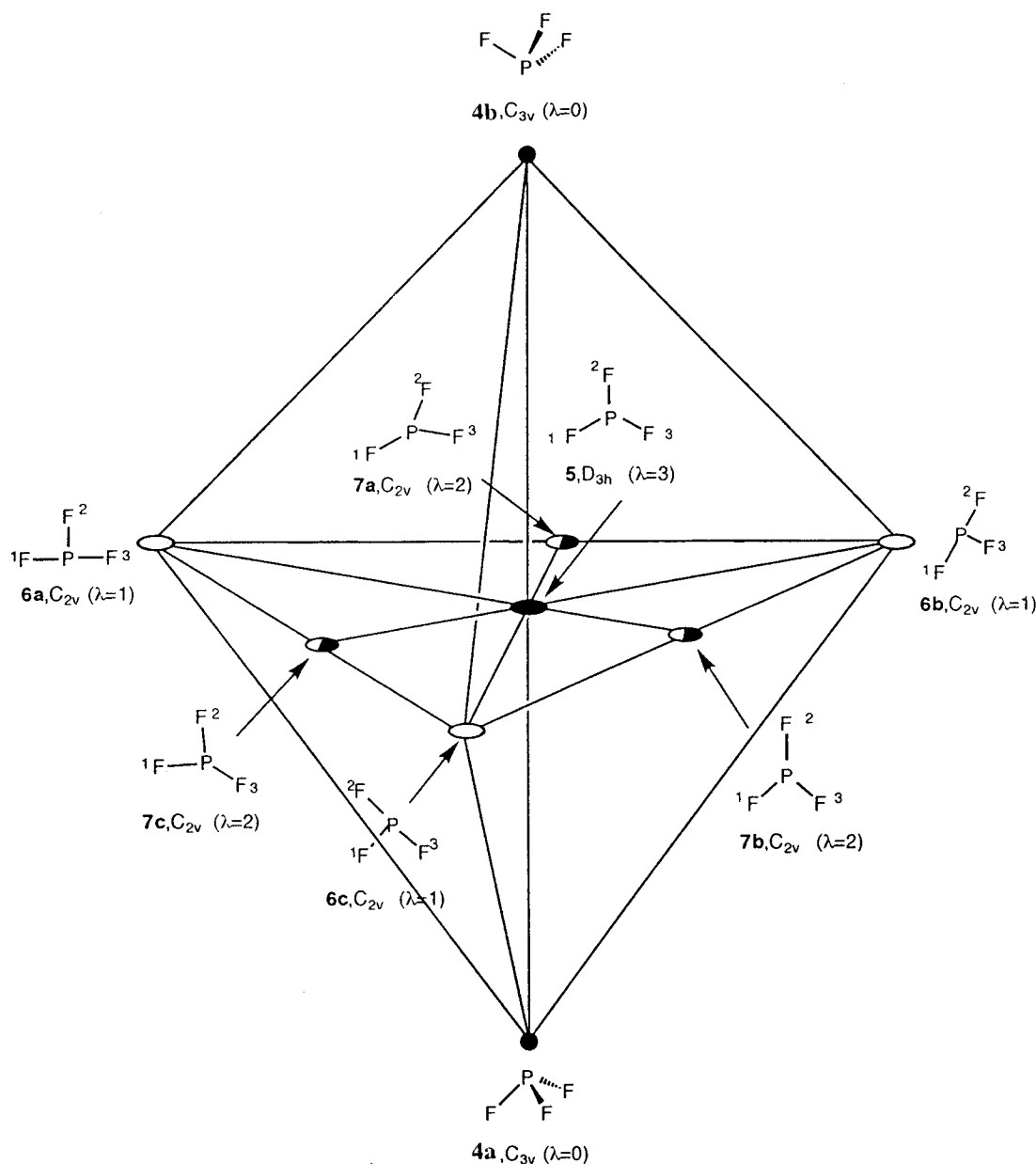
Gradient Line Reaction Paths

J. Phys. Chem. A, Vol. 101, No. 7, 1997 **1391**

Figure 13. Schematic representation of the PF_3 inversion pathways. Filled circles designate minima **4a** and **4b**. Filled, half filled, and unfilled ellipses designate the index three saddle point **5**, the index two saddle points **7a, 7b, 7c** and transition states **6a, 6b, 6c**, respectively. Solid lines represent the corresponding gradient lines connecting these points.

molecules would probably exhibit a topology similar to that of the planar PF_3 rearrangement.

Internal Inversion Pathway in PF_3

The total inversion pathway (gradient line reaction path) of PF_3 consists of three equivalent paths passing through three equivalent transition states **6a, 6b,** and **6c**. For one of these reaction pathways, the energy profile and the evolution of the transition vector are given in Figure 11. In Figure 12 we present the evolution of the six lowest Hessian eigenvalues along the gradient lines emanating from the transition state **6a** along the transition vector toward minima **4a**. Hence, the inversion of PF_3 is essentially a multidimensional process and it should be described by at least three internal coordinates: one inversion angle and two bond angles. It is difficult to represent the PF_3 PES for inversion in only two dimensions. Here, we provide a reaction graph that shows the network topology of the gradient lines connecting all stationary points in the inversion configuration region (Figure 13).

The observed topology of the PF_3 PES seems to be the same as that for the inversion of AF_3 (A = S^+, Sb, As, Bi) compounds.

Conclusions

The gradient line reaction path of the aminoborane internal rotation consists of two equivalent gradient line paths separated in configuration space by an index two stationary point. The gradient line reaction path for the PF_3 inversion consists of three equivalent paths separated by one index three and three index two stationary points. The hindered internal rotation in aminoborane and the inversion in trifluorophosphine may proceed along these equivalent pathways with equal probabilities. Hence, the aminoborane internal rotation and the AF_3 (A = P, S^+, Sb, As, Bi) inversion are essentially multidimensional processes.

1392 *J. Phys. Chem. A, Vol. 101, No. 7, 1997*

Minyaev et al.

References and Notes

(1) Minyaev, R. M. *Int. J. Quantum Chem.* **1994**, *49*, 105.

(2) (a) Minyaev, R. M.; Wales, D. J. *Chem. Phys. Lett.* **1994**, *218*, 413. (b) Minyaev, R. M.; Wales, D. J. *J. Chem. Soc. Faraday Trans.* **1994**, *90*, 1839. (c) Minyaev, R. M.; Wales, D. J. *J. Chem. Soc. Faraday Trans* **1994**, *90*, 1831.

(3) Minyaev, R. M.; Wales, D. J. *J. Phys. Chem.* **1994**, *25*, 206.

(4) (a) Collard, K. G.; Hall, G. G. *Int. J. Quantum Chem.* **1977**, *12*, 623. (b) Pechukas, P. *J. Chem. Phys.* **1976**, *64*, 1216.

(5) Murrell, J. N.; Laidler, K. J. *Faraday Trans. Soc.* **1968**, *63*, 371.

(6) Haaland, A. *Angew. Chem., Int. Ed. Engl.* **1989**, *28*, 992.

(7) Hoffmann, R. *J. Chem. Phys.* **1964**, *40*, 2474.

(8) Maouche, B.; Gayoso, J. *Int. J. Quantum Chem.* **1983**, *23*, 891.

(9) (a) Nelson, C. R.; Kessel, D. J.; Brien, F.; Weinhold, J. *J. Org. Chem.* **1980**, *45*, 2116. (b) Bentley, T. W. *J. Org. Chem.* **1982**, *47*, 60.

(10) Gropen, O.; Seip, H. M. *Chem. Phys. Lett.* **1974**, *25*, 206.

(11) Dill, J. D.; Schleyer, P. v. R.; Pople, J. A. *J. Am. Chem. Soc.* **1975**, *97*, 3402.

(12) (a) Fjeldberg, F.; Gundersen, G.; Jonvik, T.; Seip, H. M.; Saebo, S. *Acta Chem. Scand.* **1980**, *A34*, 547. (b) Budzelar, P. H. M.; Kos, J.; Clark, T.; Schleyer, P. v. R. *Organometalics* **1985**, *4*, 429.

(13) Bonacic-Koutesky, V.; Mihl, J. *J. Am. Chem. Soc.* **1985**, *107*, 1765.

(14) Ha, K. *J. Mol. Struct. THEOCHEM.* **1986**, *136*, 165.

(15) Ortiz, J. V. *Chem. Phys. Lett.* **1989**, *156*, 489.

(16) McKee, M. L. *J. Chem. Phys.* **1992**, *96*, 5380.

(17) Allen, T. L.; Fink, W. H. *Inorg. Chem.* **1993**, *32*, 4230.

(18) Weiss, M. T.; Stranberg, M. W. P. *Phys. Rev.* **1951**, *83*, 567.

(19) Weston, R. E. *J. Am. Chem. Soc.* **1954**, *76*, 2645.

(20) Swalen, J. D.; Ibers, J. A. *J. Chem. Phys.* **1962**, *36*, 1914.

(21) Allen, L. C.; Raul, A.; Mislow, K. *Angew. Chem., Int. Ed. Engl.* **1970**, *9*, 400.

(22) Lambert, J. B. In *Topics in Stereochemistry*; Allinger, N. L., Eliel, E. L., Eds.; Wiley: New York, 1971; Vol. 6.

(23) Owen, N. L. In *Internal Rotation in Molecules*; Orville-Thomas, W. J., Ed.; Wiley: London, 1974; Chapter 6.

(24) Boldyurev, A. I.; Charkin, O. P. *Zh. Strukt. Khim.* **1985**, *26*, 158.

(25) Arduengo, A. J.; Dixon, D. A. In *Heteroatom Chemistry*; Block, E., Ed.; VCH: New York, 1990.

(26) Dixon, D. A.; Arduengo, A. J.; Fukunaga, T. *J. Am. Chem. Soc.* **1986**, *108*, 2461.

(27) Dixon, D. A.; Arduengo, A. J. *J. Am. Chem. Soc.* **1987**, *109*, 338.

(28) Dixon, D. A.; Arduengo, A. J. *J. Chem. Soc., Chem. Commun.* **1987**, 498.

(29) Dixon, D. A.; Arduengo, A. J. *Int. J. Quantum Chem. Symp.* **1988**, *N22*, 85.

(30) Arduengo, A. J.; Stewart, C. *Chem. Rev.* **1994**, *94*, 1215.

(31) Clotet, A.; Rubio, J.; Illas, F. *J. Mol. Struct.: THEOCHEM* **1988**, *164*, 351.

(32) Edgecombe, K. E. *J. Mol. Struct.: THEOCHEM* **1991**, *226*, 157.

(33) Minyaev, R. M. *J. Mol. Struct.: THEOCHEM* **1992**, *262*, 79.

(34) (a) Minyaev, R. M. *Zh. Phys. Khim.* **1993**, *67*, 1. (b) Gutsev, G. L. *J. Chem. Phys.* **1993**, *98*, 444.

(35) Moc, J.; Morokuma, K. *Inorg. Chem.* **1994**, *33*, 551.

(36) Schwerdfeger, P.; Boyd, P. D. W.; Fischer, T.; Hunt, P.; Liddell, M. *J. Am. Chem. Soc.* **1994**, *116*, 9620.

(37) Yamamoto, Y.; Chen, X.; Kojima, S.; Ohdoi, K.; Kitano, M.; Doi, Y.; Akiba, K. *J. Am. Chem. Soc.* **1995**, *117*, 3922.

(38) Hehre, W. J.; Radom, L.; Schleyer, P. v. R.; Pople, J. A. *Ab Initio Molecular Orbital Theory*; J. Wiley & Sons: New York, 1986.

(39) Amos, R. D.; Alberts, I. L.; Andrews, J. S.; Colwell, S. M.; Handy, N. C.; Jayatilaka, D.; Knowles, P. J.; Kobayashi, R.; Laming, G. J.; Lee, A. M.; Maslen, P. E.; Murray, C. W.; Palmieri, P.; Rice, J. E.; Simandiras, E. D.; Stone, A. J.; Su, M. D.; Tozer, D. J. *CADPAC6.0: The Cambridge Analytic Derivatives Package*, Issue 6.0; Cambridge, 1995.

(40) Wales, D. J.; Walsh, T. R. *J. Chem. Phys.* **1996**, *105*, 6957.

(41) Dunning, T. H., Jr. *J. Chem. Phys.* **1970**, *153*, 2823.

(42) (a) Sugie, M.; Takeo, H.; Matsumura, C. *J. Mol. Spectrosc.* **1987**, *123*, 286. (b) Greenwood, N. N.; Thomas, B. S. In *Comprehensive Inorganic Chemistry*; Bailer, J. C., Ed.; Pergamon Press: Oxford, 1973; pp 925−935. (c) Pelter, A.; Smith, K. In *Comprehensive Organic Chemistry*; Barton, D., Ollis, N. D., Eds.; Pergamon Press: Oxford, 1979; pp 925−932. (d) Barfield, P. A.; Lappert, M. F.; Lee, J. *Proc. Chem. Soc., London* **1961**, 421. (e) Imberty, D.; Jaeschke, A.; Friebulin, H. *Org. Magn. Reson.* **1970**, *2*, 271. (f) Friebolin, H.; Rensch, R.; Wendel, H. *Org. Magn. Reson.* **1976**, *8*, 287. (g) Brown, C.; Cragg, R. H.; Miller, T. J.; Smith, D. O'N. *J. Organomet. Chem.* **1983**, *244*, 209. (i) Asche, A. J., III; Klein, W.; Ronssean, R. *J. Organomet. Chem.* **1994**, *468*, 21.

(43) Gerry, M. C. L.; Lewis-Bevan, W.; Merer, A. J.; Westwood, N. P. C. *J. Mol. Spectrosc.* **1985**, *110*, 153.

(44) Thorne, L. R.; Gwin, W. D. *J. Am. Chem. Soc.* **1982**, *104*, 3822.

(45) Suewram, R. D.; Thorn, L. R. *Chem. Phys. Lett.* **1981**, *78*, 157.

(46) Totani, T.; Tori, K.; Murakami, J.; Watanabe, H. *Org. Magn. Reson.* **1971**, *3*, 627.

(47) (a) Wales, D. J. *J. Chem. Soc. Faraday Trans.* **1993**, *89*, 1305. (b) Cerjan, C. J.; Miller, W. H. *J. Chem. Phys.* **1981**, *75*, 2800. (c) Simons, J.; Jorgenson, P.; Taylor, H.; Ozment, J. *J. Phys. Chem.* **1983**, *87*, 2745. (d) O'Neal, D.; Taylor, H.; Simons, J. *J. Phys. Chem.* **1984**, *88*, 1510. (e) Banerjee, A.; Adams, N.; Simons, J.; Shepard, R. *J. Phys. Chem.* **1985**, *89*, 52. (f) Baker, J. *J. Comput. Chem.* **1986**, *7*, 385; **1987**, *8*, 563. (g) Baker, J.; Hehre, W. *J. Comput. Chem.* **1991**, *12*, 606.

(48) Sun, J.-Q.; Ruedenberg, K. *J. Chem. Phys.* **1993**, *99*, 5257, 5269.

(49) Sun, J.-Q.; Ruedenberg, K.; Atchity, G. J. *J. Chem. Phys.* **1993**, *99*, 5276.

(50) Sun, J.-Q.; Ruedenberg, K. *J. Chem. Phys.* **1994**, *100*, 6101.

(51) Christe, K. O.; Dixon, D. A.; Mercier, H. P. A.; Sanders, J. C. P.; Schrobilgen, G. J.; Wilson, W. W. *J. Am. Chem. Soc.* **1994**, *116*, 2850.

(52) Ugi, I.; Marquarding, D.; Klusacek, H.; Gillespie, P. *Acc. Chem. Res.* **1971**, *4*, 288.

(53) Minyaev, R. M. *Chem. Phys. Lett.* **1992**, *196*, 203.

(54) Schwerdtfeger, P. *J. Phys. Chem.* **1996**, *100*, 2968.

(55) Gutsev, G. L. *J. Chem. Phys.* **1993**, *98*, 444.

(56) Tschumper, G. S.; Fermann, J. T.; Schaefer, H. F., III *J. Chem. Phys.* **1996**, *104*, 3676.